Photonic realization of the (2+1)-dimensional parity anomaly

Tetsuyuki OCHIAI
Photonic Materials Unit, National Institute for Materials Science (NIMS), Tsukuba 305-0044, Japan

We present a photonic realization of the parity anomaly originally found in the (2+1)-dimensional Dirac fermion. We first derive an effective Dirac Hamiltonian around the Brillouin zone corner of triangular-, honeycomb-, and kagome-lattice photonic crystals using group theory. A topological phase transition by broken space-inversion and time-reversal symmetries is derived analytically within the effective theory on the honeycomb lattice. The phase transition is closely related to the Haldane model of the two-dimensional electron system under periodic magnetic flux, which realizes the parity anomaly in a condensed-matter system. We also derive an effective theory around the Brillouin zone center, where quadratic degeneracy in momentum space take places. The effective theory there predicts a similar phenomenon as the parity anomaly. As a result, a topologically nontrivial phase and a chiral edge state are predicted even for staggered configuration of applied magnetic flux. A numerical simulation is also presented to confirm the prediction.

PACS numbers: 42.70.Qs,73.20.-r.,61.48.De.,03.65.Vf

I. INTRODUCTION

The parity anomaly is a kind of quantum anomaly in which a parity invariance is preserved in classical theory, but is broken in quantum theory.[1,2] In the (2+1)-dimensional Dirac fermion, the parity anomaly emerges as a generation of the Hall current under vanishing magnetic flux.[3] Its contribution to the Hall conductance is $\mathrm{sgn}(m) \times e^2/(2h)$, where m is the Dirac mass. Since the Dirac mass term breaks both the parity and the time-reversal symmetry (TRS), these symmetries are expected to be recovered in the limit $m \to 0$. Nevertheless, the Hall conductance, which is odd under the parity and the time reversal, becomes nonzero in the limit. Under general assumptions, however, the Hall conductance is quantized as an integer multiple of e^2/h.[4] This integer is actually the Chern number C of the first Brillouin zone (BZ) for lattice systems and is topologically invariant.[5] Therefore, the Hall conductance due to the parity anomaly is just one half of the unit, so that the half-integer contribution of the Dirac fermion is usually hidden in real systems.

In 1988 Haldane showed that it is possible to duplicate the contribution, so that the parity anomaly can be manifest in condensed matter systems.[6] He studied a tight-binding model on the honeycomb lattice under a periodic magnetic flux with zero average per unit cell. The resulting band structure exhibits massive Dirac spectra at each corner (named either the K or K' point) of the first BZ. Therefore, the effective theory near the Fermi level lying in the mass gap is described by two Dirac fermions around the K and K' points. The physical origin of the Dirac mass is the broken space-inversion symmetry (SIS) and the broken TRS. The interplay between the two broken symmetries results in a nontrivial topological phase diagram of the Haldane model.

It seems that the parity anomaly is a quantum effect and that no classical counterpart exists. However, this is not true. The underlying physics of the parity anomaly is that the Dirac fermion has the Berry phase of $\pm\pi$ for a closed loop around the zero momentum in the limit of $m \to 0$.[7] Note that the Chern number roughly corresponds to the Berry phase divided by 2π. The Berry phase emerges in a variety of waves including the Schrödinger (de Brogie) wave,[8] light wave,[9,10] acoustic wave,[11] spin wave,[12] and so on. Therefore, if the Dirac-type spectrum emerges in these waves, it is possible to exhibit a similar phenomenon as the parity anomaly. In fact, Haldane and Raghu showed that a triangular-lattice photonic crystal (PhC) with the Dirac spectrum exhibits the nonzero Chern number by a TRS breaking.[13] Later, this idea is generalized to a square-lattice PhC with quadratic degeneracy, where the nonzero Chern number also emerges by a TRS breaking.[14,15] Other types of PhC and photonic lattices made of photorefractive crystals can also have Dirac spectra,[16,17] suggesting that an optical analog of the parity anomaly also works.

For various applications such as nonreciprocal transport, it is important to control the topology. In the original Haldane model, the TRS- and SIS-breaking parameters give rise to this controllability. By changing one of the parameters, two bands touch and separate, resulting in the abrupt change of the Chern number. Inspired by this work, the author and his collaborator showed numerically that the Dirac "masses" around K and K' are controllable in honeycomb-lattice PhCs by the magneto-optical effect (TRS breaking) and the refractive-index contrast between the two sublattices (SIS breaking).[18] A similar idea was explored for anisotropic triangular-lattice PhCs.[19] The phase diagram in the two-parameter space of the broken symmetries exhibits a topological phase transition as in the Haldane model. However, the phase diagram is derived only numerically, and its theoretical foundation was still lacking.

Furthermore, effects of broken symmetries are still unclear around the Γ point of the honeycomb lattice, as well as for the other related lattices such as the kagome lattice. The band topology is not simply determined by some properties around the K and K' point. The Γ point also can affect the topology. Therefore, a detailed analysis of

the broken symmetries around the Γ point is necessary to describe the topological phase transition. From the viewpoint of spatial symmetry, triangular, honeycomb, and kagome lattices are categorized to the same class that can have the C_{6v} point group. Therefore, a unified description is available in these lattices. The phase space becomes richer in this order, and a nontrivial topology in the honeycomb lattice can appear in a more complex manner in the kagome lattice. Thus, an analysis of one of these triangular-like lattices is helpful to study the other lattices.

In this paper we present a detailed theoretical analysis of the topological phase transition in triangular-like PhCs. The analysis is based on the effective Hamiltonians with the aid of group theory. We first consider unperturbed PhCs that have the C_{6v} point group. These include triangular-, honeycomb-, and kagome-lattice PhCs of identical cylinders. This point group allows double degeneracy in the energy levels at the Γ, K, and K' points of the first BZ. Then, we take account of the $\boldsymbol{k}\cdot\boldsymbol{p}$ perturbation and the perturbation of broken symmetries. The point group symmetry of the unperturbed system determines the possible form of the effective Hamiltonian for the perturbed system. In particular, the Dirac Hamiltonian is derived for the degenerate modes at the K and K' points. This Hamiltonian is closely related to that of the Haldane model, and exhibits a nontrivial phase diagram. As for the Γ point, the effective Hamiltonian that is quadratic in momentum is derived. The Hamiltonian predicts a topologically nontrivial phase and a chiral edge state even for a staggered configuration of applied magnetic flux. Such a phase is forbidden in the effective theory around K and K', and is derived for the first time in photonic system. A direct evidence of the nontrivial topology is also presented by numerical simulation.

This paper is organized as follows. In Sec. II we derive the effective Dirac Hamiltonian around the K and K' points, and the analytic phase diagram is obtained. The results are compared with the numerical phase diagram that was obtained previously. Section III is devoted to presenting the effective theory around the Γ point. A nontrivial topology in a staggered configuration of the applied magnetic flux is predicted. In Sec. IV the nontrivial topology and a chiral edge state are demonstrated by numerical simulation. The results agree with the theoretical prediction. Finally, our summary and discussion are given.

II. EFFECTIVE HAMILTONIAN AROUND K AND K'

Let us formulate the effective Dirac Hamiltonian around the K and K' points. The Maxwell equation for tensor permittivity $\overleftrightarrow{\epsilon}$ and permeability $\overleftrightarrow{\mu}$ is given by

$$\boldsymbol{\nabla}\times[\overleftrightarrow{\xi}(\boldsymbol{x})\boldsymbol{\nabla}\times\boldsymbol{E}(\boldsymbol{x})]=\frac{\omega^2}{c^2}\overleftrightarrow{\epsilon}(\boldsymbol{x})\boldsymbol{E}(\boldsymbol{x}), \tag{1}$$

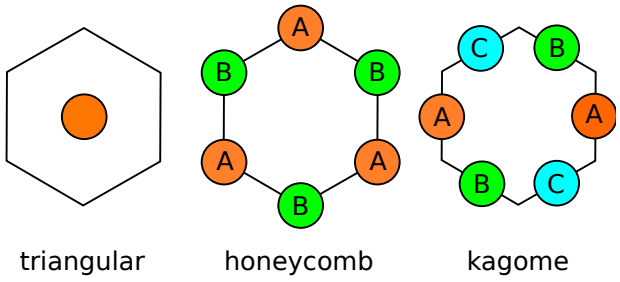

FIG. 1. (Color online) The triangular-like photonic crystals composed of circular cylinders. The hexagon is a unit cell of the lattices.

$$\boldsymbol{\nabla}\times[\overleftrightarrow{\eta}(\boldsymbol{x})\boldsymbol{\nabla}\times\boldsymbol{H}(\boldsymbol{x})]=\frac{\omega^2}{c^2}\overleftrightarrow{\mu}(\boldsymbol{x})\boldsymbol{H}(\boldsymbol{x}). \tag{2}$$

Here, tensors $\overleftrightarrow{\xi}$ and $\overleftrightarrow{\eta}$ are the inverse permeability and the inverse permittivity, respectively. In the following, we assume a rotationally symmetric form with respect to the z axis for these tensors:

$$\overleftrightarrow{\theta}=\begin{pmatrix}\theta_{xx} & \theta_{xy} & 0\\ -\theta_{xy} & \theta_{xx} & 0\\ 0 & 0 & \theta_z\end{pmatrix}\quad(\theta=\epsilon,\mu,\eta,\xi). \tag{3}$$

We also assume that they are dispersion free. In a two-dimensional PhC of circular cylinders, the momentum k_z parallel to the cylindrical axis (z axis) is conserved. Here, we restrict $k_z=0$. The system is decoupled into the transverse-electric (TE) and the transverse-magnetic (TM) polarizations because of the inversion symmetry $z\to -z$.

Let us focus on the TM polarization. The TE polarization can be dealt with in a parallel way. In terms of the plane-wave expansion, the z component of Eq. (1) is written as

$$\sum_{\boldsymbol{g}'}H_{\boldsymbol{g}\boldsymbol{g}'}e_{\boldsymbol{g}'}=\frac{\omega^2}{c^2}\sum_{\boldsymbol{g}'}K_{\boldsymbol{g}\boldsymbol{g}'}e_{\boldsymbol{g}'}, \tag{4}$$

$$H_{\boldsymbol{g}\boldsymbol{g}'}=\xi_{\boldsymbol{g}-\boldsymbol{g}'}(\boldsymbol{k}+\boldsymbol{g})\cdot(\boldsymbol{k}+\boldsymbol{g}') +\mathrm{i}\zeta_{\boldsymbol{g}-\boldsymbol{g}'}[(\boldsymbol{k}+\boldsymbol{g})\times(\boldsymbol{k}+\boldsymbol{g}')]_z, \tag{5}$$

$$K_{\boldsymbol{g}\boldsymbol{g}'}=(\epsilon_z)_{\boldsymbol{g}-\boldsymbol{g}'}, \tag{6}$$

$$E_z(\boldsymbol{x})=\sum_{\boldsymbol{g}}\mathrm{e}^{\mathrm{i}(\boldsymbol{k}+\boldsymbol{g})\cdot\boldsymbol{x}}e_{\boldsymbol{g}}, \tag{7}$$

$$\theta(\boldsymbol{x})=\sum_{\boldsymbol{g}}\mathrm{e}^{\mathrm{i}\boldsymbol{g}\cdot\boldsymbol{x}}\theta_{\boldsymbol{g}}\quad(\theta=\xi,\zeta,\epsilon_z). \tag{8}$$

Here, $\xi_{xx}\equiv\xi$, $\xi_{xy}\equiv\mathrm{i}\zeta$, $\boldsymbol{k}$ is the two-dimensional (2d) Bloch momentum, and $\boldsymbol{g}$ is a 2d reciprocal lattice vector. A schematic illustration of the system under study is shown in Fig. 1. The first BZ is depicted in Fig. 2. As the unperturbed system we assume $A=B$ for the honeycomb lattice and $A=B=C$ for the kagome lattice (see Fig. 1). We also assume the off-diagonal component θ_{xy} of the permittivity and the permeability tensors is zero. The systems thus have the

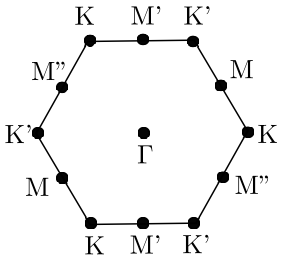

FIG. 2. The first Brillouin zone of the triangular-like lattices. Points of high symmetry are indicated.

$C_{6v}(\equiv \{1, 2C_6, 2C_3, C_2, 3\sigma_x, 3\sigma_y\})$ point-group symmetry. Here, C_n stands for $2\pi/n$ rotation, and $\sigma_{x(y)}$ is the parity transformation $x(y) \to -x(y)$. Accordingly, the modes at the K and K' points are classified by the irreducible representations of $C_{3v}(\equiv \{1, 2C_3, 3\sigma_y\})$, which is the $\boldsymbol{k}$ group there. Let us pick up a doubly-degenerate E mode of C_{3v} at the K point of the unperturbed system. It satisfies

$$\sum_{\boldsymbol{g}'} H^{(0)}_{\boldsymbol{g}\boldsymbol{g}'} e^{(p)}_{\boldsymbol{g}'} = \frac{\omega_0^2}{c^2} \sum_{\boldsymbol{g}'} K^{(0)}_{\boldsymbol{g}\boldsymbol{g}'} e^{(p)}_{\boldsymbol{g}} \quad (p = 1, 2), \tag{9}$$

$$H^{(0)}_{\boldsymbol{g}\boldsymbol{g}'} = \xi^{\rm av}_{\boldsymbol{g}-\boldsymbol{g}'}(\boldsymbol{k}_{\rm K} + \boldsymbol{g}) \cdot (\boldsymbol{k}_{\rm K} + \boldsymbol{g}'), \tag{10}$$

$$K^{(0)}_{\boldsymbol{g}\boldsymbol{g}'} = (\epsilon_z^{\rm av})_{\boldsymbol{g}-\boldsymbol{g}'}. \tag{11}$$

Here, $\xi^{\rm av}$ and $\epsilon_z^{\rm av}$ are the C_{6v} symmetric part of the corresponding functions, and are defined latter. The two eigenstates $e^{(p)}_{\boldsymbol{g}}$ $(p = 1, 2)$ form the E representation of C_{3v} and thus satisfy

$$e^{(p)}_{G^{-1}(\boldsymbol{g}-\boldsymbol{g}_0)} = \sum_{q=1,2} e^{(q)}_{\boldsymbol{g}} D_{qp}(G). \tag{12}$$

Here, G is an element of C_{3v} with $G\boldsymbol{k}_{\rm K} = \boldsymbol{k}_{\rm K} + \boldsymbol{g}_0$, and $D(G)$ is a unitary representation of the E mode. Without the loss of generality, we put $\boldsymbol{k}_{\rm K} = (4\pi/(3a), 0)$, where a is the lattice constant. We normalize the basis as

$$\sum_{\boldsymbol{g}\boldsymbol{g}'} (e^{(p)}_{\boldsymbol{g}})^* K^{(0)}_{\boldsymbol{g}\boldsymbol{g}'} e^{(q)}_{\boldsymbol{g}'} = \delta_{pq}. \tag{13}$$

A positive definite $K^{(0)}$ matrix is assumed.

From now on, we focus on a honeycomb lattice PhC that consists of A and B triangular sublattices of the circular cylinders, embedded in a background medium of diagonal permeability μ_b and z component of permittivity ϵ_{zb}. The radii of the A and B cylinders are taken to be the same. The triangular and kagome lattices are discussed in Appendices. We consider the $\boldsymbol{k}\cdot\boldsymbol{p}$ perturbation and the perturbation of broken symmetries from the E mode at K. Thus, the expansion parameters are 1) the deviation of the $\boldsymbol{k}$ vector from the K point,

$$\delta\boldsymbol{k} \equiv \boldsymbol{k} - \boldsymbol{k}_{\rm K}, \tag{14}$$

2) the deviation of ξ and ϵ_z from $A = B$,

$$\delta\theta \equiv \frac{1}{2}(\theta_A - \theta_B) \quad (\theta = \xi, \epsilon_z), \tag{15}$$

and 3) the magnitude of the magneto-optical effect of the A and B cylinders, ζ_A and ζ_B. Thus, $\xi(\boldsymbol{x})$ and $\epsilon_z(\boldsymbol{x})$ (represented by $\theta(\boldsymbol{x})$) are given by

$$\begin{aligned}\theta(\boldsymbol{x}) &= \theta_b + (\theta_A - \theta_b)S^A(\boldsymbol{x}) + (\theta_B - \theta_b)S^B(\boldsymbol{x}) \\ &= \theta^{\rm av}(\boldsymbol{x}) + \delta\theta(S^A(\boldsymbol{x}) - S^B(\boldsymbol{x})),\end{aligned} \tag{16}$$

$$\theta^{\rm av}(\boldsymbol{x}) \equiv \theta_b + (\theta_a - \theta_b)(S^A(\boldsymbol{x}) + S^B(\boldsymbol{x})), \tag{17}$$

being $\theta_a \equiv (\theta_A + \theta_B)/2$. Function $\zeta(\boldsymbol{x})$ is given by

$$\zeta(\boldsymbol{x}) = \zeta_A S^A(\boldsymbol{x}) + \zeta_B S^B(\boldsymbol{x}). \tag{18}$$

Here, $S^{A(B)}(\boldsymbol{x})$ is a periodic function that is zero inside the $A(B)$ cylinder and zero otherwise.

The degenerate-perturbation theory up to the first order in these expansion parameters results in the diagonalization of the following effective Hamiltonian:

$$\mathcal{H}_{pq} = \mathcal{H}^{(k)}_{pq} + \mathcal{H}^{(\xi)}_{pq} + \mathcal{H}^{(\epsilon)}_{pq} + \mathcal{H}^{(\zeta)}_{pq}, \tag{19}$$

$$\mathcal{H}^{(\beta)}_{pq} = \sum_{\boldsymbol{g}\boldsymbol{g}'} (e^{(p)}_{\boldsymbol{g}})^* H^{(\beta)}_{\boldsymbol{g}\boldsymbol{g}'} e^{(q)}_{\boldsymbol{g}'}, \tag{20}$$

$$H^{(k)}_{\boldsymbol{g}\boldsymbol{g}'} = \xi^{\rm av}_{\boldsymbol{g}-\boldsymbol{g}'}\delta\boldsymbol{k} \cdot (2\boldsymbol{k}_{\rm K} + \boldsymbol{g} + \boldsymbol{g}'), \tag{21}$$

$$H^{(\xi)}_{\boldsymbol{g}\boldsymbol{g}'} = \delta\xi(S^A_{\boldsymbol{g}-\boldsymbol{g}'} - S^B_{\boldsymbol{g}-\boldsymbol{g}'})(\boldsymbol{k}_{\rm K} + \boldsymbol{g}) \cdot (\boldsymbol{k}_{\rm K} + \boldsymbol{g}'), \tag{22}$$

$$H^{(\epsilon)}_{\boldsymbol{g}\boldsymbol{g}'} = -\frac{\omega_0^2}{c^2}\delta\epsilon_z(S^A_{\boldsymbol{g}-\boldsymbol{g}'} - S^B_{\boldsymbol{g}-\boldsymbol{g}'}), \tag{23}$$

$$H^{(\zeta)}_{\boldsymbol{g}\boldsymbol{g}'} = {\rm i}(\zeta_A S^A_{\boldsymbol{g}-\boldsymbol{g}'} + \zeta_B S^B_{\boldsymbol{g}-\boldsymbol{g}'})[(\boldsymbol{k}_{\rm K} + \boldsymbol{g}) \times (\boldsymbol{k}_{\rm K} + \boldsymbol{g}')]_z \tag{24}$$

Here, $\mathcal{H}^{(k)}$ is the $\boldsymbol{k}\cdot\boldsymbol{p}$ perturbation, $\mathcal{H}^{(\xi)}$ and $\mathcal{H}^{(\epsilon)}$ are the perturbation of the broken SIS, and $\mathcal{H}^{(\zeta)}$ is the perturbation of the broken TRS. Factor $S^{A(B)}_{\boldsymbol{g}}$ is the Fourier transform of $S^{A(B)}(\boldsymbol{x})$. The diagonalization problem now becomes

$$\sum_{q=1,2} \mathcal{H}_{pq} c_q = \mathcal{E} c_p, \tag{25}$$

$$e_{\boldsymbol{g}} = \sum_{p=1,2} c_p e^{(p)}_{\boldsymbol{g}}, \tag{26}$$

$$\frac{\omega^2}{c^2} = \frac{\omega_0^2}{c^2} + \mathcal{E}. \tag{27}$$

Using the point group symmetry of C_{3v}, we can show that

$$\mathcal{H}^{(k)}(\delta\boldsymbol{k}) = D^\dagger(G)\mathcal{H}^{(k)}(G\delta\boldsymbol{k})D(G) \quad (G \in C_{3v}), \tag{28}$$

$$\mathcal{H}^{(\beta)} = D^\dagger(C_3)\mathcal{H}^{(\beta)}D(C_3) \quad (\beta = \xi, \epsilon, \zeta), \tag{29}$$

$$\mathcal{H}^{(\beta)} = -D^\dagger(\sigma_y)\mathcal{H}^{(\beta)}D(\sigma_y) \quad (\beta = \xi, \epsilon). \tag{30}$$

As for $\mathcal{H}^{(\zeta)}$, we divide it into $\zeta_A\mathcal{H}^{(\zeta A)} + \zeta_B\mathcal{H}^{(\zeta B)}$. We can easily show that

$$\mathcal{H}^{(\zeta A)} = -D^\dagger(\sigma_y)\mathcal{H}^{(\zeta B)}D(\sigma_y). \tag{31}$$

By employing the unitary representation for $D(G)$ given in Appendix C, we obtain

$$\mathcal{H}^{(k)} = \lambda_k(\sigma_3\delta k_x - \sigma_1\delta k_y), \tag{32}$$

$$\mathcal{H}^{(\xi)} = \lambda_\xi\delta\xi\sigma_2, \tag{33}$$

$$\mathcal{H}^{(\epsilon)} = \lambda_\epsilon\delta\epsilon_z\sigma_2, \tag{34}$$

$$\mathcal{H}^{(\zeta)} = \lambda^+_\zeta(\zeta_A + \zeta_B)\sigma_2 + \lambda^-_\zeta(\zeta_A - \zeta_B)\hat{1}, \tag{35}$$

where $\sigma_i (i = 1, 2, 3)$ is the Pauli matrix, and $\hat{1}$ is the 2 by 2 unit matrix. Summing up all the terms, we have the following effective Hamiltonian around K:

$$\mathcal{H}_{\rm K} = \lambda_k(\sigma_3\delta k_x - \sigma_1\delta k_y) + M_{\rm K}\sigma_2 + \lambda_\zeta^-(\zeta_A - \zeta_B)\hat{1}, \quad (36)$$

$$M_{\rm K} = \lambda_\xi\delta\xi + \lambda_\epsilon\delta\epsilon_z + \lambda_\zeta^+(\zeta_A + \zeta_B). \quad (37)$$

This is a Hamiltonian of the massive Dirac fermion. The eigenvalue of the effective Hamiltonian is thus

$$\mathcal{E}_{\rm K} = \lambda_\zeta^-(\zeta_A - \zeta_B) \pm \sqrt{\lambda_k^2|\delta\boldsymbol{k}|^2 + M_{\rm K}^2}. \quad (38)$$

Next, let us consider the K' point. The K and K' points are related by the inversion of the $\boldsymbol{k}$ vector. By using the inversion transformation, we can show

$$\mathcal{H}_{\rm K'}^{(\beta)} = -\mathcal{H}_{\rm K}^{(\beta)} \quad (\beta = k, \xi, \epsilon), \quad (39)$$

$$\mathcal{H}_{\rm K'}^{(\zeta)} = \lambda_\zeta^+(\zeta_A + \zeta_B)\sigma_2 - \lambda_\zeta^-(\zeta_A - \zeta_B)\hat{1}. \quad (40)$$

Therefore, the effective Dirac Hamiltonian around K' becomes

$$\mathcal{H}_{\rm K'} = -\lambda_k(\sigma_3\delta k_x - \sigma_1\delta k_y) + M_{\rm K'}\sigma_2 - \lambda_\zeta^-(\zeta_A - \zeta_B)\hat{1}, \quad (41)$$

$$M_{\rm K'} = -\lambda_\xi\delta\xi - \lambda_\epsilon\delta\epsilon_z + \lambda_\zeta^+(\zeta_A + \zeta_B). \quad (42)$$

The eigenvalue becomes

$$\mathcal{E}_{\rm K'} = -\lambda_\zeta^-(\zeta_A - \zeta_B) \pm \sqrt{\lambda_k^2|\delta\boldsymbol{k}|^2 + M_{\rm K'}^2}. \quad (43)$$

The minus sign of the first term in Eq. (41) is absorbed in the redefinition of $\delta\boldsymbol{k}$. Compared to the effective Hamiltonian around K, the energy shifts in an opposite way and the mass term is different.

A naive evaluation of the Chern number gives the sum of the contribution of two Dirac *photons* around the K and K' points.[31] At each K and K', there emerges the parity anomaly. Therefore, we obtain

$$C = \pm\frac{1}{2}(\mathrm{sgn}(M_{\rm K}) + \mathrm{sgn}(M_{\rm K'})), \quad (44)$$

which has an integer, either 0 or ± 1. Let us put $\delta\xi = 0$ and $\zeta_A = \zeta_B = \zeta$. Then, the two-parameter space spanned by $\delta\epsilon_z$ and ζ has the phase diagram of Fig. 3, regarding the Chern number. At the phase boundary either $M_{\rm K}$ or $M_{\rm K'}$ is zero.

Some comments are needed on the above results. First, the Dirac mass changes its sign depending on the magnitudes of $\delta\xi$, $\delta\epsilon_z$, ζ_A, and ζ_B. Second, if a staggered magnetic flux is applied for the A and B cylinders, namely $\zeta_A = -\zeta_B$, it does not affect the Dirac mass, but shifts the energy. In this case, we have $M_{\rm K} = -M_{\rm K'}$, resulting in a cancellation of the parity anomaly between K and K'. The Chern number thus vanishes. Therefore, the staggered configuration of the applied magnetic flux does not permit the nontrivial topology within the effective theory. This result is consistent with the fact that in the staggered configuration the C_{3v} symmetry is preserved if $\delta\xi = \delta\epsilon_z = 0$. Third, the above derivation of the effective Dirac Hamiltonian can be easily extended to other systems. The key equations are the symmetry properties given in Eqs. (28)–(31), from which the Dirac Hamiltonian is analytically derived. The derivation shows a striking contrast to that in the tight-binding model of graphene.[21] In the latter system the Dirac Hamiltonian is derived from the tight-binding one simply by the Taylor expansion on the pseudo-spin basis.

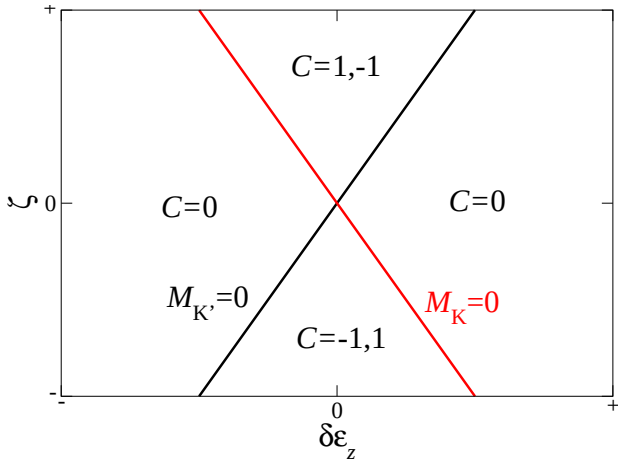

FIG. 3. (Color online) The phase diagram spanned by $\delta\epsilon_z$ (the degree of the broken space-inversion symmetry) and $\zeta (\equiv \zeta_A = \zeta_B)$ (the degree of the broken time-reversal symmetry) for the honeycomb-lattice photonic crystal.

Previously, the author and his collaborator studied numerically a topological phase transition in the TM polarization of a honeycomb lattice PhC.[18] There, we focused on the lowest (in frequency) Dirac point at K and K' as the unperturbed system. By numerical diagonalization of the unperturbed system, we can obtain eigenvector $e_{\boldsymbol{g}}^{(p)}$ at the degenerate mode. The parameters of the effective Dirac Hamiltonian are then available by Eqs. (32-35). To examine this Hamiltonian, we compare the shift of the eigenfrequencies both in the effective theory and in numerical diagonalization of the perturbed system. The results are shown in Fig. 4. We can see a nice agreement of the results if the perturbation is small enough. However, it exhibits a substantial difference for large perturbation. Thus, the gap opening and closing in a small perturbation range, and the resulting topology change are correctly described by the effective Hamiltonian. Actually, the parameters of the effective Hamiltonian shown in Fig. 4 reproduce the topological phase diagram of Ref. 18 fairly well.

III. EFFECTIVE HAMILTONIAN AROUND Γ

Next, we consider another source of topological phase transition. That is, the Γ point. Concerning the degeneracy there, the honeycomb lattice shows a remarkable contrast to the triangular and kagome lattices. In the

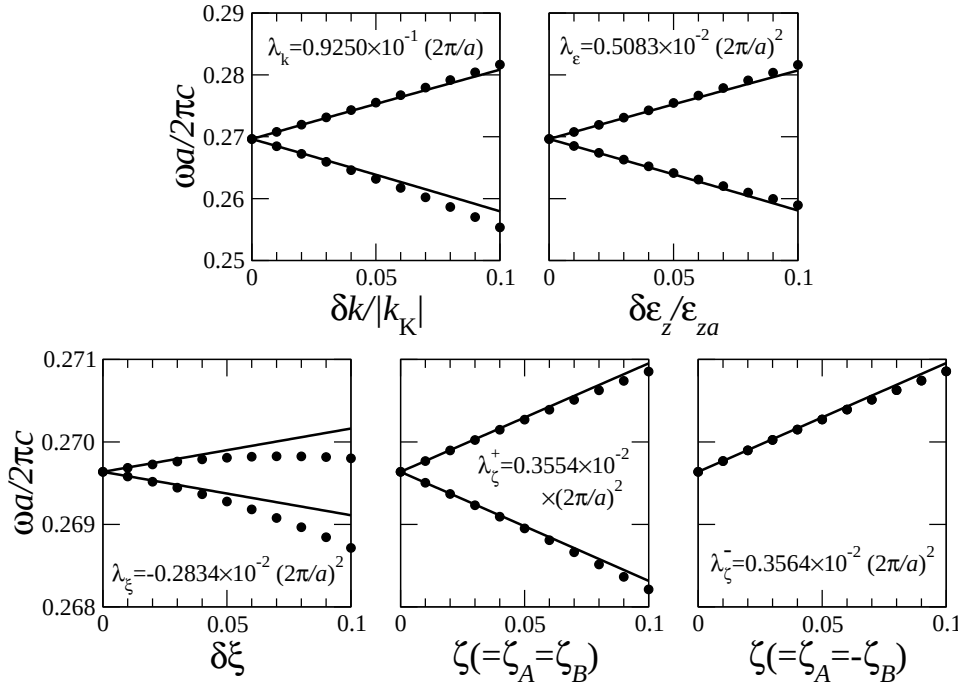

FIG. 4. Comparison of the eigenfrequency shift of a doubly degenerate mode at the K point in a honeycomb-lattice photonic crystal. The unperturbed system consists of identical circular cylinders with radius $0.2a$, permittivity $\epsilon_{za} = 12$, and diagonal permeability $\mu_{xx} = 1$, embedded in air. The TM polarization is assumed. Solid line stands for the results of the effective theory with the parameters taken from the unperturbed eigenvector through Eqs. (32)–(35). Dot represents the results of numerical diagonalization of the Maxwell equation. In the top-left panel $\delta\boldsymbol{k}$ is directed from K to Γ.

honeycomb lattice, the degeneracy at the Γ point is not lifted by the perturbation of the broken SIS, $A \neq B$. In terms of group theory, this statement corresponds to the fact that the E_1 and E_2 representations of C_{6v} are compatible with the E representation of C_{3v}, which is the point group of the honeycomb lattice with $A \neq B$. On the other hand, in the triangular and kagome lattices, the symmetry-breaking perturbation immediately lifts the degeneracy. In this section we focus on the honeycomb lattice and regard the unperturbed system as that having the $C_{3v}(\equiv \{1, 2C_3, 3\sigma_x\})$ point group. The remaining perturbations are that of $\boldsymbol{k}\cdot\boldsymbol{p}$ and that of the TRS breaking. We should note that the C_{3v} symmetry here is different from the C_{3v} symmetry of the $\boldsymbol{k}$ group at K and K' discussed in Sec. II. The latter symmetry does not include σ_x, but includes σ_y. The effective Hamiltonians of the triangular and kagome lattices are given in the appendices.

Since the Γ point is the time-reversal invariant $\boldsymbol{k}$ point, we need to consider this symmetry as well as C_{3v}. The TRS prohibits the Dirac-type Hamiltonian, which is linear in $\boldsymbol{k}$. To see this property, let us consider the first-order $\boldsymbol{k}\cdot\boldsymbol{p}$ perturbation for a degenerate E mode. The relevant Hamiltonian is given by

$$\mathcal{H}^{(k)}_{pq} = \sum_{\boldsymbol{g}\boldsymbol{g}'} (e^{(p)}_{\boldsymbol{g}})^* \xi_{\boldsymbol{g}-\boldsymbol{g}'} \boldsymbol{k}\cdot(\boldsymbol{g}+\boldsymbol{g}') e^{(q)}_{\boldsymbol{g}'}. \tag{45}$$

Now, $e^{(p)}_{\boldsymbol{g}}$ $(p = 1, 2)$ is the eigenvectors of the E mode at the Γ point. The symmetry property of $e^{(p)}_{\boldsymbol{g}}$ becomes

$$e^{(p)}_{G^{-1}\boldsymbol{g}} = \sum_{q=1,2} e^{(q)}_{\boldsymbol{g}} D_{qp}(G). \tag{46}$$

Therefore, the first-order Hamiltonian satisfies

$$\mathcal{H}^{(k)}_{pq}(\boldsymbol{k}) = \sum_{p'q'} [D^\dagger(G)]_{pp'} \mathcal{H}^{(k)}_{p'q'}(G\boldsymbol{k}) [D(G)]_{q'q}, \tag{47}$$

for $G \in C_{3v}$. The above equation results in

$$\mathcal{H}^{(k)}_{pq} = \lambda_k [k_x\sigma_1 + k_y\sigma_3]_{pq}, \tag{48}$$

using the representation given in Appendix C. Besides, the TRS of the unperturbed system implies

$$(e^{(p)}_{-\boldsymbol{g}})^* = \sum_{q=1,2} e^{(q)}_{\boldsymbol{g}} U_{qp}, \tag{49}$$

with $U^\dagger U = 1$. The compatibility between the symmetry operation Eq. (46) and the TRS relation Eq. (49) yields $D(G)U = UD^*(G)$. Since the representation matrix can be real, the unitary matrix U commutes with $D(G)$ for any G. By Schur's lemma, matrix U has to be the unit matrix times a phase factor.[22] As a result, the TRS of the unperturbed system yields $(\mathcal{H}^{(k)}_{pq})^* = -\mathcal{H}^{(k)}_{pq}$. Therefore, we obtain $\lambda_k = 0$; i.e., $\mathcal{H}^{(k)}_{pq} = 0$.

Accordingly, we need to employ the second-order $\boldsymbol{k}\cdot\boldsymbol{p}$ perturbation as in the Luttinger-Kohn model.[23] The effective Hamiltonian of $\boldsymbol{k}\cdot\boldsymbol{p}$ now becomes

$$\mathcal{H}^{(k^2)}_{pq} = |\boldsymbol{k}|^2 \sum_{\boldsymbol{g}\boldsymbol{g}'} (e^{(p)}_{\boldsymbol{g}})^* \xi_{\boldsymbol{g}-\boldsymbol{g}'} e^{(q)}_{\boldsymbol{g}'} + \sum_{n\neq p,q} \frac{c^2}{\omega_0^2-\omega_n^2} \mathcal{H}^{(k)}_{pn}\mathcal{H}^{(k)}_{nq}. \quad (50)$$

Here, index n refers to the eigenstates other than the degenerate modes concerned. By symmetry consideration, we have

$$\mathcal{H}^{(k^2)}_{pq}(\boldsymbol{k}) = \sum_{p'q'} [D^\dagger(G)]_{pp'} \mathcal{H}^{(k^2)}_{p'q'}(G\boldsymbol{k}) [D(G)]_{q'q}. \quad (51)$$

From the above constraint we obtain the possible form of the effective Hamiltonian as

$$\mathcal{H}^{(k^2)} = \lambda^{(1)}_{k^2}|\boldsymbol{k}|^2\hat{1} + \lambda^{(2)}_{k^2}(\sigma_3(k_x^2-k_y^2)+2\sigma_1 k_x k_y). \quad (52)$$

The above equation is obtained either by expanding as $\mathcal{H}^{(k^2)} = \mathcal{H}^{(xx)}k_x^2 + \mathcal{H}^{(yy)}k_y^2 + \mathcal{H}^{(xy)}k_xk_y$ and applying Eq. (51) or by deducing the possible forms of the matrix elements $\mathcal{H}^{(k)}_{pn}$ with intermediate states n being classified according to the irreducible representations of C_{3v}. For instance, intermediate A_1 and A_2 modes give rise to the terms proportional to

$$\begin{pmatrix} k_x^2 & k_xk_y \\ k_xk_y & k_y^2 \end{pmatrix} \quad \text{and} \quad \begin{pmatrix} k_y^2 & -k_xk_y \\ -k_xk_y & k_x^2 \end{pmatrix}, \quad (53)$$

respectively. A linear combination of these two terms is written as Eq. (52).

Next, let us consider the first-order perturbation of the TRS breaking. The relevant Hamiltonian is written as

$$\mathcal{H}^{(\zeta)} = \zeta_A \mathcal{H}^{(\zeta A)} + \zeta_B \mathcal{H}^{(\zeta B)}, \quad (54)$$

$$\mathcal{H}^{(\zeta\alpha)} = \sum_{\boldsymbol{g}\boldsymbol{g}'} (e^{(p)}_{\boldsymbol{g}})^* \mathrm{i} S^\alpha_{\boldsymbol{g}-\boldsymbol{g}'} (\boldsymbol{g}\times\boldsymbol{g}')_z e^{(q)}_{\boldsymbol{g}'} \quad (\alpha = A, B) \quad (55)$$

The spatial symmetry under C_{3v} results in

$$\mathcal{H}^{(\zeta\alpha)} = D^\dagger(C_3)\mathcal{H}^{(\zeta\alpha)}D(C_3), \quad (56)$$

$$\mathcal{H}^{(\zeta\alpha)} = -D^\dagger(\sigma_x)\mathcal{H}^{(\zeta\alpha)}D(\sigma_x). \quad (57)$$

We obtain the following form of $\mathcal{H}^{(\zeta)}$,

$$\mathcal{H}^{(\zeta)} = \Lambda_\zeta \sigma_2, \quad (58)$$

$$\Lambda_\zeta = \lambda^A_\zeta \zeta_A + \lambda^B_\zeta \zeta_B. \quad (59)$$

This form is consistent with the TRS of the unperturbed system: $(\mathcal{H}^{(\zeta)})^* = -\mathcal{H}^{(\zeta)}$. We should note that if $A = B$ in the unperturbed system, $\lambda_{\zeta A} = \lambda_{\zeta B}$ is derived. The other terms up to the second order in the expansion parameters $\boldsymbol{k}$, ζ_A, and ζ_B in the Lödwin perturbation scheme are given by

$$\mathcal{H}^{(k\zeta)}_{pq} = \sum_{\boldsymbol{g}\boldsymbol{g}'} (e^{(p)}_{\boldsymbol{g}})^* \mathrm{i}\zeta_{\boldsymbol{g}-\boldsymbol{g}'} (\boldsymbol{k}\times(\boldsymbol{g}'-\boldsymbol{g}))_z e^{(q)}_{\boldsymbol{g}'} + \sum_{n\neq p,q} \frac{c^2}{\omega_0^2-\omega_n^2} (\mathcal{H}^{(k)}_{pn}\mathcal{H}^{(\zeta)}_{nq} + \mathcal{H}^{(\zeta)}_{pn}\mathcal{H}^{(k)}_{nq}), \quad (60)$$

$$\mathcal{H}^{(\zeta^2)}_{pq} = \sum_{n\neq p,q} \frac{c^2}{\omega_0^2-\omega_n^2} \mathcal{H}^{(\zeta)}_{pn}\mathcal{H}^{(\zeta)}_{nq}. \quad (61)$$

By symmetry consideration, we obtain

$$\mathcal{H}^{(k\zeta)} = \Lambda_{k\zeta}(k_x\sigma_3 - k_y\sigma_1), \quad (62)$$

$$\mathcal{H}^{(\zeta^2)} = \Lambda_{\zeta^2}\hat{1}, \quad (63)$$

$$\Lambda_{k\zeta} = \lambda^A_{k\zeta}\zeta_A + \lambda^B_{k\zeta}\zeta_B, \quad (64)$$

$$\Lambda_{\zeta^2} = \lambda^A_{\zeta^2}\zeta_A^2 + \lambda^B_{\zeta^2}\zeta_B^2 + \lambda^{AB}_{\zeta^2}\zeta_A\zeta_B. \quad (65)$$

Summing up all the terms, the effective Hamiltonian around Γ becomes

$$\mathcal{H}_\Gamma = \hat{1}\left(\lambda^{(1)}_{k^2}|\boldsymbol{k}|^2 + \Lambda_{\zeta^2}\right) + \sigma_2\Lambda_\zeta + \sigma_3\left(\lambda^{(2)}_{k^2}(k_x^2-k_y^2) + \Lambda_{k\zeta}k_x\right) + \sigma_1\left(\lambda^{(2)}_{k^2}2k_xk_y - \Lambda_{k\zeta}k_y\right), \quad (66)$$

and the energy spectrum becomes

$$\mathcal{E}_\Gamma = \lambda^{(1)}_{k^2}|\boldsymbol{k}|^2 + \Lambda_{\zeta^2} \pm \sqrt{\left(\lambda^{(2)}_{k^2}\right)^2|\boldsymbol{k}|^4 + \Lambda^2_{k\zeta}|\boldsymbol{k}|^2 + 2\lambda^{(2)}_{k^2}\Lambda_{k\zeta}k_x(k_x^2-3k_y^2) + \Lambda^2_\zeta}. \quad (67)$$

Therefore, in this approximation, the band dispersion is no longer isotropic in momentum space, but is three-fold rotationally symmetric. We can easily check that factor $k_x(k_x^2-3k_y^2)$ is invariant under C_3. This three-fold symmetry is a direct consequence of the point group in the perturbed system, which consists of $\{1, C_3, C_3^2\}$. The bands are gapped with gap width $2|\Lambda_\zeta|$ at the zero momentum. In this case the Berry phase of the two bands for a circular loop around the zero momentum is shown to be $2\pi\mathrm{sgn}(\Lambda_\zeta)$, provided $|\Lambda_\zeta|, |\Lambda_{k\zeta}|k_0 \ll |\lambda^{(2)}_{k^2}|k_0^2$.[15] Here, k_0 is the circle radius in the momentum space. A similar Berry phase is obtained in bilayer graphene.[24] This formula explains a topological phase transition in a certain honeycomb-lattice PhC.

Suppose that two photonic bands are touched quadratically only at the Γ point in the unperturbed system. When the TRS is broken in the perturbed system, the gap opens. At the same time, the two bands acquire the

nonzero Chern numbers as

$$C = \pm \mathrm{sgn}(\Lambda_\zeta), \tag{68}$$

in a naive evaluation. Note that the Berry phase divided by 2π corresponds to the Chern number. We should recall that Λ_ζ corresponds to the magneto-optical coupling. The above formula indicates that even if the magneto-optical coupling, which breaks both the parity and the TRS, is almost vanishing, the Chern number is still nonzero. This statement is analogous to the parity anomaly of the 2+1-dimensional Dirac fermion, although the band dispersion is quadratic.

An interesting remark is that even in the staggered configuration of the magneto-optical effect, i.e., $\zeta_A = -\zeta_B$, it is possible to exhibits the nontrivial topology. This provides a striking contrast to the effective theory around the K and K' points. There, the staggered configuration just shifts the energy, but the mass gap does not open. As a result, the topology change is prohibited. In the next section, we confirm numerically that the topology change takes place in the staggered configuration.

IV. CHIRAL EDGE STATES UNDER A STAGGERED MAGNETIC FIELD

In this section we present numerical evidences of the nontrivial topology in a staggered configuration of the magneto-optical effect. Let us consider the honeycomb-lattice PhC composed of magneto-optical cylinders. The TM polarization is considered here. In the TM polarization the magneto-optical effect emerges through the off-diagonal part of the permeability tensor. In a simple spin model of ferrimagnetic materials,[25] the permeability tensor at frequencies $\omega \gg \omega_0, \omega_m$ behaves as $\mu_{xx} = \mu_{yy} \simeq 1$ and $\mu_{xy} = -\mu_{yx} \simeq -\mathrm{i}\omega_m/\omega$. Here, ω_0 and ω_m are the Larmor and the saturation-magnetization frequencies, respectively. Since ω_m is typically in the GHz range, we consider (sub)THz frequency regions and put $\omega_m/\omega = \pm 0.01$ for simplicity. As the SIS breaking, we assume the permittivity contrast between A and B cylinders as $\epsilon_{zA} = 14$ and $\epsilon_{zB} = 10$. The radii of the A and B cylinders are kept fixed as $r_A = r_B = 0.2a$, where a is the lattice constant (period of each sublattice).

The photonic band structure of the honeycomb-lattice PhC is shown in Fig. 5. We point out that in the unperturbed system the fifth and the sixth bands are in contact solely at the Γ point, and that they are well separated from the other bands. By introducing the magneto-optical effect in a staggered configuration $\zeta_A = -\zeta_B \simeq -0.01$, the two bands separate a bit as shown in the right panel. We can check that the gap width is proportional to $|\zeta_A| = |\zeta_B|$.[32]

According to the effective theory, the gap opening is accompanied by the topology change. As a result, the chiral edge state should emerge by the so-called bulk-edge correspondence.[27] To verify this statement, we study the edge states in the system. The edge states relevant to

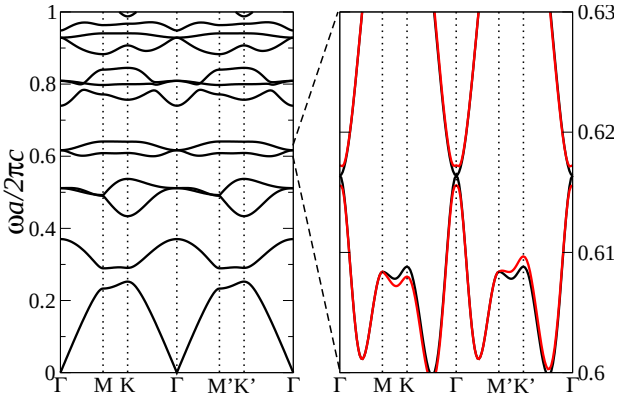

FIG. 5. (Color online) The photonic band structure of the TM polarization in the honeycomb-lattice photonic crystal composed of A and B cylinders embedded in air. The permittivity of the A and B cylinders are 14 and 10, respectively. The radius of the cylinders is kept fixed as to be $0.2a$, where a is the lattice constant of A and B sublattices. Left panel: The photonic band structure of the system with the time-reversal symmetry. The permeability tensor of the A and B cylinders is set to be unity. Right panel: Enlarged view of the fifth and the sixth bands for the system with the time-reversal symmetry (black curve) and the system without the time-reversal symmetry (red curve). In the latter system, the permeability tensor is taken to be $\mu_{xy} = -\mu_{yx} = 0.01\mathrm{i}$ for the A cylinders, and $\mu_{xy} = -\mu_{yx} = -0.01\mathrm{i}$ for the B cylinders (staggered configuration). The remaining diagonal components are 1.

the gap lie inside the light cone ($\omega > c|k_\parallel|$), so that it leaks from the PhC by coupling with the radiation modes of continuous spectrum. Although such a leaky edge state with complex eigenfrequencies can be shown to exist numerically, we restrict ourselves to a finite-width PhC sandwiched by metal. In such a case the edge state is truly guided and has real eigenfrequencies.

Let us consider a stripe-shaped PhC of the honeycomb lattice sandwiched by a metal. Metals at THz frequencies can be well approximated by the perfect electric conductor. A schematic illustration of the PhC stripe is shown in Fig. 6. Figure 7 shows the dispersion relation of the edge states localized in zigzag and armchair edges of the honeycomb-lattice PhC without the TRS.

Since the PhC has a stripe shape, two types of the edge states, localized in upper and lower edges, can exist in the pseudo-gap (i.e., $\boldsymbol{k}$-dependent gap). In both the types, the dispersion curves of the edge states traverse the pseudo-gap and terminate at the different bands (taking into account that the periodicity of the parallel momentum $k_\parallel$). These properties are inherent in the relevant bulk bands with a nontrivial topology by the bulk-edge correspondence. Let us have a close look at the omnidirectional gap region ($0.6155 < \omega a/(2\pi c) < 0.617$). The zigzag edge there support one upper-edge state (indicated by **c** in Fig. 7) and three lower-edge states (indicated by **a**, **b**, and **d**). The upper-edge state has a negative group velocity and there is no other counter-propagating edge

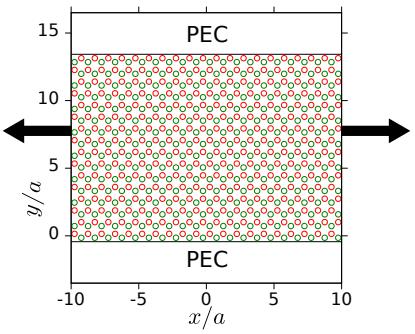

FIG. 6. (Color online) A schematic illustration of the photonic-crystal stripe under consideration. The case of the zigzag edge is shown. The photonic crystal has infinite extent in the x direction and has 16-layer thickness in the y direction, sandwiched by the perfect electric conductor (PEC). Red (green) circles stand for the $A(B)$ cylinders.

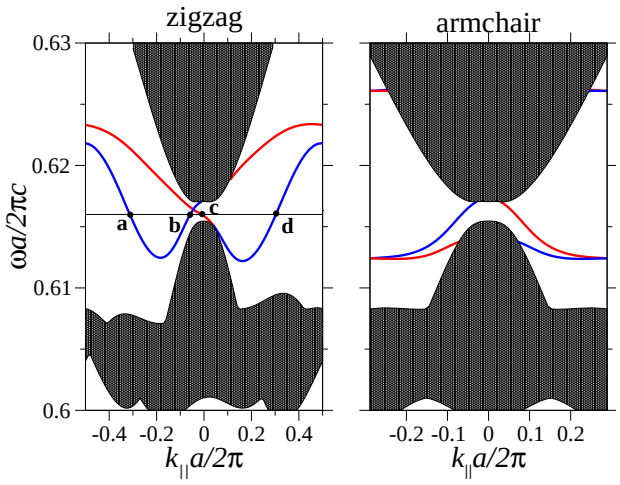

FIG. 7. (Color online) The dispersion relation of the edge states in the finite-thick (16 layers) photonic crystal sandwiched by the perfect electric conductor. The edge states localized in the upper (lower) edge are represented by red (blue) curve. The projected band structure is also plotted. The shaded region corresponds to the bulk-band region, and the blank region is the pseudo gap. The honeycomb-lattice photonic crystal without the time-reversal symmetry is assumed and the same physical parameters as in the right panel of Fig. 5 were used. Symbol $k_\parallel$ refers to the Bloch momentum parallel to the edges.

state localized in the upper edge. Such an edge state is called chiral (one-way) and is robust against disorder. As for the lower edge, states **b** and **d** have positive group velocities, and state **a** has a negative one. Thus, there is an excess of the positively-propagating edge states. If disorder is introduced in the system, the three states mix with each other. However, the excess gives rise to a perfectly conducting channel as in graphene ribbons.[28]

The electric field intensity $|E_z|^2$ of the edge state at

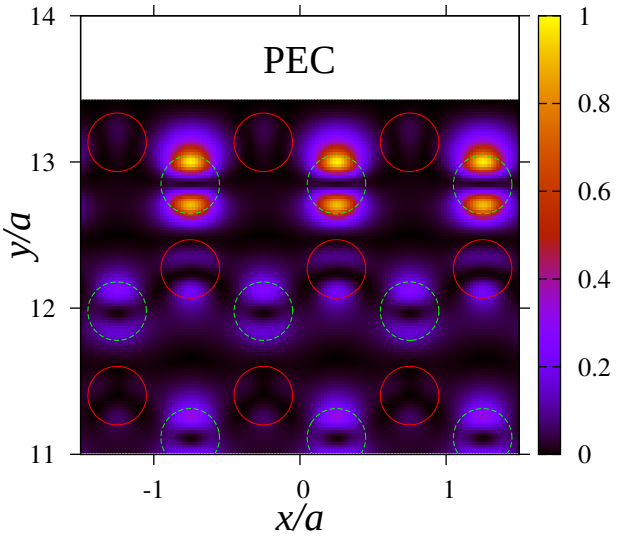

FIG. 8. (Color online) The electric field intensity $|E_z|^2$ of the zigzag edge state at **c** ($k_\parallel a/2\pi = -0.01$) in Fig. 7. The edge state is localized in the upper zigzag edge. Red (green) circle stands for the $A(B)$ cylinders. The intensity is normalized by the maximum intensity.

c is plotted in Fig. 8. We can see the electric field is localized almost in the B cylinders of the boundary layer. A node is clearly visible inside the B cylinder, suggesting that the p-wave Mie resonance of the B cylinder affects strongly the edge state. In fact the nearest (in frequency) resonance can be found at $\omega a/(2\pi c) = 0.5734$ for the isolated B cylinders with $\overleftrightarrow{\mu} = 1$. Its full width at half maximum covers the edge-state frequency. The next nearest is at $\omega a/(2\pi c) = 0.4883$ for the isolated A cylinders with $\overleftrightarrow{\mu} = 1$. The small off-diagonal components of $\mu_{xy} = -\mu_{yx} = \pm 0.01\mathrm{i}$ change the resonance frequencies just by 0.2%. A considerable amount of the field intensity persists in the region far from the boundary. This is because the band gap is narrow and the edge state is close in frequency to the bulk bands.

As for the armchair edge, the upper and lower edge states are obviously chiral (one-way) in the omnidirectional gap region. The group-velocity flow of the edge states are common in the zigzag and armchair edges. Namely, the upper edge states flow negatively (from right to left), whereas the lower edge modes flow positivity (from left to right). Thus, a counter-clockwise flow is realized in the omnidirectional gap. We should note that there are another armchair edge states around $\omega a/2\pi c = 0.625$ outside the omnidirectional gap. They are nearly degenerate although not clearly visible. Actually, there are two curves (red and blue) both for positive and negative $k_\parallel$ regions. However, their dispersion curves are terminated in the same band, and thus these edge states are irrelevant to the nontrivial topology.

As an independent check of the effective theory, we also evaluated the Chern number numerically by the BZ

integral.[18] We obtain $C = 1$ for the lower (in frequency) band and $C = -1$ for the upper band. The results are consistent with the flow of the chiral edge states.

Finally, let us comment on a possible experimental observation of the predicted effect. As noted, we assume two kinds of ferrimagnetic cylinders placed in a honeycomb lattice with lattice constant on the order of several hundred microns. This length scale is derived from $\omega a/(2\pi c) \sim 0.6$, $\omega_m/\omega = \pm 0.01$, and ω_m typically in several GHz. A direct measurement of the chiral edge state can be made with a pointlike or linelike source and receivers such as THz dipole antenna. If a source is placed near the edge, the light emitted from it can propagate in a unidirectional manner along the edge. One of the two receivers placed left and right of the source along the edge can detect the uni-directional propagation. The other receiver keeps silent. If the magnetization of the ferrimagnetic rods is reversed, the emitted light propagates in the opposite direction. Therefore, the roles of the two receivers are interchanged.

V. SUMMARY AND DISCUSSION

In summary, we have presented effective Hamiltonians in triangular-like PhCs having C_{6v} point group symmetry as the zeroth order approximation. The $\boldsymbol{k}\cdot\boldsymbol{p}$ perturbation and the perturbation of the broken symmetries are taken into account. The effective Dirac Hamiltonian around the BZ corner is derived analytically. It predicts the topological phase transition for honeycomb-lattice PhCs. The predicted phase diagram agrees quite well with the numerical phase diagram obtained previously. The effective Hamiltonian around the center of the BZ is also derived. The Hamiltonian predicts a topological phase transition even for a staggered configuration of the applied magnetic flux. The resulting nontrivial topology is numerically verified by the existence of the chiral edge states via the bulk-edge correspondence, and by the numerical calculation of the Chern number.

In this paper we have presented effective theories around degenerate points in triangular-like PhCs by group theory. It is noteworthy that our derivation of the effective Hamiltonian does not rely on the analytic expression of the eigenstates for the full Hamiltonian as in the tight-binding model, nor on any phenomenological ansatz. The derivation is simply based on group theory. Therefore, the method is easily extended to any system of C_{6v} point-group symmetry as the unperturbed system, irrespective of system details, either bosonic or fermionic.

In addition, the present formalism can be applied also to the systems with accidental degeneracy at high-symmetry points in the first BZ. Recently, Huang *et al.* showed that the accidental degeneracy at the Γ point results in a Dirac-type spectrum intersected by a quadratic one.[29] To obtain the accidental degeneracy, we need a fine-tuning of the physical parameters, such that the frequency of a non-degenerate mode coincides with that of a degenerate mode. Such a system acts as a novel metamaterial with zero refractive index. Thus, it will be important to explore the effects of broken symmetries and detuning.

Another important issue is a way to introduce broken symmetries. In this paper we pick up the index contrast between the A and B cylinders for the honeycomb lattice and the magneto-optical effect as the perturbation of broken symmetries. However, sources of broken symmetry are not limited in these two perturbations. There are many ways to break the system symmetry, such as lattice distortion, TE-TM coupling, and optical absorption. Among them, the radius contrast between A and B will be important from the viewpoint of experiment. The index contrast and the radius contrast have their own merits and demerits. Although the radius contrast can be implemented more easily in the fabrication processes, the index contrast allows us to tune it dynamically. We should also mention that the relevant Hamiltonian of the radius contrast has the same form as of the index contrast, because the spatial symmetry of the relevant Hamiltonians is the same. Therefore, if we replace $\delta\epsilon_z$ with $\delta r \equiv (r_A - r_B)/2$ in Fig. 3, a similar phase diagram is obtained. Moreover, the topology change and the chiral edge states discussed in Secs. III and IV are allowed even if the unperturbed system does not have the index contrast, but has the radius contrast.

Finally, let us comment on the similarity and difference in the parity anomaly between electronic and photonic systems. As noted in the Introduction, the parity anomaly in electronic systems is the generation of the Hall current under vanishing magnetic flux. The Hall current and the Hall conductance of Ce^2/h are directly measured. On the other hand in photonic systems, the Hall current and the Hall conductance are ill defined, and thus the Chern number of the parity anomaly [Eqs. (44) and (68)] is not directly measured. Instead, the bulk-edge correspondence implies the emergence of the chiral edge states as in electronic systems, which can be physically observed.

Further difference in the parity anomaly between electronic and photonic systems can be found in their dimensionality. The 2+1-dimensional Dirac fermion refers to the planar fermion confined in plane. On the other hand, the two-dimensional PhC under study has infinite extent in the z direction and the relevant eigenstates are extended uniformly in this direction. Although the dimensionality is different between the two systems, they both possess the parity anomaly in common as a consequence of the Dirac spectrum. The mode confinement around the edge also highlights a contrast between the two systems. In electronic systems, chiral edge states due to the bulk-edge correspondence are always confined with the work function. In photonic systems, they are not generally confined because of the leakage of the edge states into the radiation continuum outside PhC. To prevent the leakage in photonic systems, in this paper we employ the perfect electric conductor wall as in Fig. 6.

However, even if the leakage exists, the bulk-edge correspondence of the parity anomaly still holds as shown in Ref. 18.

We hope this paper stimulates further investigation of the parity anomaly and relevant symmetry-breaking physics in photonic systems.

Appendix A: triangular lattice

Let us summarize the results for a triangular lattice. In the triangular lattice composed of circular cylinders, we consider the effective Hamiltonian around a doubly degenerate E mode at K and K'. The $\boldsymbol{k}\cdot\boldsymbol{p}$ perturbation and the perturbation of the broken TRS are taken into account. Let us denote the magneto-optical coupling of the cylinders as ζ_a. The effective Hamiltonian in the linear order of $\delta\boldsymbol{k}$ and ζ_a becomes

$$\mathcal{H}_{\mathrm{K(K')}} = \tau_3\lambda_k(\sigma_3\delta k_x - \sigma_1\delta k_y) + \lambda_\zeta\zeta_a\sigma_2, \quad \text{(A1)}$$

where τ_3 is the valley spin, namely, $\tau_3 = 1$ for K and $\tau_3 = -1$ for K'. This is a massive Dirac Hamiltonian with mass $\lambda_\zeta\zeta_a$. The mass term does not change its sign between K and K' points. Therefore, the Chern number becomes

$$C = \pm\mathrm{sgn}(\lambda_\zeta\zeta_a), \quad \text{(A2)}$$

provided that the two bands touch solely at K and K' in the unperturbed system. The $\pm$ sign refers to the upper and lower bands. Since ζ_a is proportional to the applied magnetic field, it corresponds to the sign of magnetic field.

At the Γ point, there are two kinds of double degeneracy, the E_1 and E_2 modes in the unperturbed system with the C_{6v} point group. In both the cases, the effective Hamiltonian up to the second order in $\boldsymbol{k}$ and ζ_a becomes

$$\begin{aligned}\mathcal{H}_\Gamma = &\left(\lambda^{(1)}_{k^2}|\boldsymbol{k}|^2 + \lambda_{\zeta^2}\zeta_a^2\right)\hat{1} + \lambda_\zeta\zeta_a\sigma_2 \\ &+\lambda^{(2)}_{k^2}(\sigma_3(k_x^2 - k_y^2) + 2\sigma_1 k_x k_y). \quad \text{(A3)}\end{aligned}$$

Note that the terms proportional to $k_i\zeta_a$ vanish by the SIS. The Chern number is the same in its expression as Eq. (A2), if the two bands touch solely at the Γ point in the unperturbed system.

Appendix B: kagome lattice

Next, we consider a kagome-lattice PhC that consists of A, B, and C triangular sublattices of circular cylinders. A doubly degenerate E mode emerges at the K and K' points if A, B, and C cylinders are identical. Around the degenerate point, we consider the perturbation in the linear order of $\delta\boldsymbol{k}$, $\delta\xi_\alpha$, $\delta\epsilon_{z\alpha}$, and ζ_α ($\alpha = A, B, C$) with

$$\delta\theta_\alpha \equiv \theta_\alpha - \theta_a, \quad \text{(B1)}$$

$$\theta_a \equiv \frac{1}{3}(\theta_A + \theta_B + \theta_C) \quad (\theta = \xi, \epsilon_z). \quad \text{(B2)}$$

The effective Hamiltonian becomes

$$\begin{aligned}\mathcal{H}_{\mathrm{K(K')}} &= \tau_3\lambda_k(\sigma_3\delta k_x - \sigma_1\delta k_y) \\ &+\lambda_\xi\left(-\sigma_3\frac{3}{2}(\delta\xi_B + \delta\xi_C) + \sigma_1\frac{\sqrt{3}}{2}(\delta\xi_B - \delta\xi_C)\right) \\ &+\lambda_\epsilon\left(-\sigma_3\frac{3}{2}(\delta\epsilon_{zB} + \delta\epsilon_{zC}) + \sigma_1\frac{\sqrt{3}}{2}(\delta\epsilon_{zB} - \delta\epsilon_{zC})\right) \\ &+\lambda_\zeta(\zeta_A + \zeta_B + \zeta_C)\sigma_2. \quad \text{(B3)}\end{aligned}$$

Note that the terms proportional to $\delta\xi_\alpha$ or $\delta\epsilon_{z\alpha}$ are absorbed in the redefinition of $\delta\boldsymbol{k}$:

$$\mathcal{H}_{\mathrm{K(K')}} = \tau_3\lambda_k(\sigma_3\widetilde{\delta k_x} - \sigma_1\widetilde{\delta k_y}) + \sigma_2 M, \quad \text{(B4)}$$

$$M \equiv \lambda_\zeta(\zeta_A + \zeta_B + \zeta_C), \quad \text{(B5)}$$

$$\begin{aligned}\widetilde{\delta k_x} \equiv \delta k_x &- \tau_3\frac{\lambda_\xi}{\lambda_k}\frac{3}{2}(\delta\xi_B + \delta\xi_C) \\ &-\tau_3\frac{\lambda_\epsilon}{\lambda_k}\frac{3}{2}(\delta\epsilon_{zB} + \delta\epsilon_{zC}), \quad \text{(B6)}\end{aligned}$$

$$\begin{aligned}\widetilde{\delta k_y} \equiv \delta k_y &- \tau_3\frac{\lambda_\xi}{\lambda_k}\frac{\sqrt{3}}{2}(\delta\xi_B - \delta\xi_C) \\ &-\tau_3\frac{\lambda_\epsilon}{\lambda_k}\frac{\sqrt{3}}{2}(\delta\epsilon_{zB} - \delta\epsilon_{zC}). \quad \text{(B7)}\end{aligned}$$

Therefore, a massive Dirac spectrum is obtained with respect to shifted momentum $\widetilde{\delta\boldsymbol{k}}$. The Chern number now becomes the sum over of the two Dirac photons localized around the momenta slightly shifted from K and K'. The result is simply given by

$$C = \pm\mathrm{sgn}(\lambda_\zeta(\zeta_A + \zeta_B + \zeta_C)), \quad \text{(B8)}$$

provided that the two bands touch solely at K and K' in the unperturbed system.

Around the Γ point, the effective Hamiltonian up to the second order is given by

$$\begin{aligned}\mathcal{H}_\Gamma &= \lambda^{(1)}_{k^2}|\boldsymbol{k}|^2\hat{1} + \lambda^{(2)}_{k^2}(\sigma_3(k_x^2 - k_y^2) + 2\sigma_1 k_x k_y) \\ &+\lambda_\xi\left(-\sigma_3\frac{3}{2}(\delta\xi_B + \delta\xi_C) + \sigma_1\frac{\sqrt{3}}{2}(\delta\xi_B - \delta\xi_C)\right) \\ &+\lambda_\epsilon\left(-\sigma_3\frac{3}{2}(\delta\epsilon_{zB} + \delta\epsilon_{zC}) + \sigma_1\frac{\sqrt{3}}{2}(\delta\epsilon_{zB} - \delta\epsilon_{zC})\right) \\ &+\lambda_\zeta(\zeta_A + \zeta_B + \zeta_C)\sigma_2, \quad \text{(B9)}\end{aligned}$$

for both the E_1 and E_2 modes. Note that the cross terms of $k_i\delta\xi_\alpha$, $k_i\delta\epsilon_{z\alpha}$, and $k_i\zeta_\alpha$ vanish by the SIS. We also note the quadratic terms composed of $\delta\xi_\alpha$, $\delta\epsilon_{z\alpha}$, and ζ_α are nonzero, but are neglected for simplicity. In this case the terms proportional to $\delta\xi_\alpha$ or $\delta\epsilon_{z\alpha}$ cannot be absorbed in the redefinition of $\boldsymbol{k}$. As a result, the equifrequency curve is not isotropic around the Γ point, but is invariant under $\boldsymbol{k}$ to $-\boldsymbol{k}$. The Berry phase for a closed circular loop with radius k_0 around the zero momentum is given by $\theta_B = \pm 2\pi\mathrm{sgn}(\lambda_\zeta(\zeta_A + \zeta_B + \zeta_C))$, provided $|\lambda_\xi\delta\xi_\alpha|, |\lambda_\epsilon\delta\epsilon_{z\alpha}|, |\lambda_\zeta\zeta_\alpha| \ll |\lambda^{(2)}_{k^2}|k_0^2$. Thus, the same Chern number in its expression as Eq. (B8) is obtained, if the two bands touch solely at the Γ point in the unperturbed system.

Appendix C: representation matrices

Here, we summarize the representation matrices used in the paper. We assume the following matrices for the E representation of the $C_{3v}(=\{1, 2C_3, 3\sigma_y\})$ $\boldsymbol{k}$ group at K(or K'):

$$D_E(C_3) = \begin{pmatrix} -\frac{1}{2} & -\frac{\sqrt{3}}{2} \\ \frac{\sqrt{3}}{2} & -\frac{1}{2} \end{pmatrix}, \quad D_E(\sigma_y) = \begin{pmatrix} 1 & 0 \\ 0 & -1 \end{pmatrix} \tag{C1}$$

As for the E representation of the $C_{3v}(=\{1, 2C_3, 3\sigma_x\})$ point group at the Γ point, we assume

$$D_E(C_3) = \begin{pmatrix} -\frac{1}{2} & -\frac{\sqrt{3}}{2} \\ \frac{\sqrt{3}}{2} & -\frac{1}{2} \end{pmatrix}, \quad D_E(\sigma_x) = \begin{pmatrix} -1 & 0 \\ 0 & 1 \end{pmatrix} \tag{C2}$$

Obviously, the above representations are orthogonal, and thus unitary.

The E_1 and E_2 representations of the $C_{6v}(=\{1, 2C_6, 2C_3, C_2, 3\sigma_x, 3\sigma_y\})$ point group of the unperturbed triangular and kagome lattices at the Γ point are given by

$$\begin{aligned} D_{E_1}(C_6) &= \begin{pmatrix} \frac{1}{2} & -\frac{\sqrt{3}}{2} \\ \frac{\sqrt{3}}{2} & \frac{1}{2} \end{pmatrix}, \quad D_{E_1}(\sigma_x) = \begin{pmatrix} -1 & 0 \\ 0 & 1 \end{pmatrix}, \\ D_{E_1}(C_3) &= \begin{pmatrix} -\frac{1}{2} & -\frac{\sqrt{3}}{2} \\ \frac{\sqrt{3}}{2} & -\frac{1}{2} \end{pmatrix}, \quad D_{E_1}(\sigma_y) = \begin{pmatrix} 1 & 0 \\ 0 & -1 \end{pmatrix}, \\ D_{E_1}(C_2) &= \begin{pmatrix} -1 & 0 \\ 0 & -1 \end{pmatrix}, \end{aligned} \tag{C3}$$

$$\begin{aligned} D_{E_2}(C_6) &= \begin{pmatrix} -\frac{1}{2} & \frac{\sqrt{3}}{2} \\ -\frac{\sqrt{3}}{2} & -\frac{1}{2} \end{pmatrix}, \quad D_{E_2}(\sigma_x) = \begin{pmatrix} -1 & 0 \\ 0 & 1 \end{pmatrix}, \\ D_{E_2}(C_3) &= \begin{pmatrix} -\frac{1}{2} & -\frac{\sqrt{3}}{2} \\ \frac{\sqrt{3}}{2} & -\frac{1}{2} \end{pmatrix}, \quad D_{E_2}(\sigma_y) = \begin{pmatrix} -1 & 0 \\ 0 & 1 \end{pmatrix}, \\ D_{E_2}(C_2) &= \begin{pmatrix} 1 & 0 \\ 0 & 1 \end{pmatrix}. \end{aligned} \tag{C4}$$

Since the E_1 representation basis behaves like (x, y), its representation matrices are easily derived. On the contrary, the E_2 representation basis behaves like $(xy, x^2 - y^2)$. Therefore, naive representation matrices by the basis become, for instance,

$$\tilde{D}_{E_2}(C_6) = \begin{pmatrix} -\frac{1}{2} & -\frac{\sqrt{3}}{4} \\ -\sqrt{3} & -\frac{1}{2} \end{pmatrix}, \tag{C5}$$

which is not unitary. To make the matrices unitary, we perform the similarity transformation as

$$D_{E_2} = V^{-1}\tilde{D}_{E_2}V, \quad V = \begin{pmatrix} 1 & 0 \\ 0 & 2 \end{pmatrix}, \tag{C6}$$

resulting in Eq. (C4).

ACKNOWLEDGMENTS

This work was supported by KAKENHI (Grant No. 23540380) of Japan Society for the Promotion of Science.

[1] A. J. Niemi and G. W. Semenoff, Phys. Rev. Lett. **51**, 2077 (1983)
[2] A. N. Redlich, Phys. Rev. D **29**, 2366 (1984)
[3] G. W. Semenoff, Phys. Rev. Lett. **53**, 2449 (1984)
[4] J. E. Avron, R. Seiler, and B. Simon, Phys. Rev. Lett. **51**, 51 (1983)
[5] D. J. Thouless, M. Kohmoto, M. P. Nightingale, and M. den Nijs, Phys. Rev. Lett. **49**, 405 (1982)
[6] F. D. M. Haldane, Phys. Rev. Lett. **61**, 2015 (1988)
[7] T. Ando, T. Nakanishi, and R. Saito, J. Phys. Soc. Jpn. **67**, 2857 (1998)
[8] M. V. Berry, Proc. Roy. Soc. London Ser. A **392**, 45 (1984)
[9] A. Tomita and R. Y. Chiao, Phys. Rev. Lett. **57**, 937 (1986)
[10] M. Onoda, S. Murakami, and N. Nagaosa, Phys. Rev. Lett. **93**, 083901 (2004)
[11] K. Y. Bliokh and V. D. Freilikher, Phys. Rev. B **74**, 174302 (2006)
[12] Q. Niu and L. Kleinman, Phys. Rev. Lett. **80**, 2205 (1998)
[13] F. D. M. Haldane and S. Raghu, Phys. Rev. Lett. **100**, 013904 (2008)
[14] Z. Wang, Y. D. Chong, J. D. Joannopoulos, and M. Soljačić, Phys. Rev. Lett. **100**, 013905 (2008)
[15] Y. D. Chong, X. G. Wen, and M. Soljačić, Phys. Rev. B **77**, 235125 (2008)
[16] J. Bravo-Abad, J. D. Joannopoulos, and M. Soljačić, Proc. Natl. Acad. Sci. USA **109**, 9761 (2012)
[17] O. Peleg, G. Bartal, B. Freedman, O. Manela, M. Segev, and D. N. Christodoulides, Phys. Rev. Lett. **98**, 103901 (2007)
[18] T. Ochiai and M. Onoda, Phys. Rev. B **80**, 155103 (2009)
[19] S. Raghu and F. D. M. Haldane, Phys. Rev. A **78**, 033834 (2008)
[20] This "local" procedure does not correctly take account of the entire first Brillouin zone, which is two-torus. See discussions in Ref. 30
[21] P. R. Wallace, Phys. Rev. **71**, 622 (1947)
[22] T. Inui, Y. Tanabe, and Y. Onodera, *Group Theory and its Applications in Physics* (Springer, 1996)
[23] J. M. Luttinger and W. Kohn, Phys. Rev. **97**, 869 (1955)
[24] K. S. Novoselov, E. McCann, S. V. Morozov, V. I. Fal'ko, M. I. Katsnelson, U. Zeitler, D. Jiang, F. Schedin, and A. K. Geim, Nature Physics **2**, 177 (2006)
[25] D. M. Pozar, *Microwave Engineering* (Wiley-India, 2009)
[26] For completeness, the parameters of the effective Hamiltonian are $\lambda^{(1)}_{k^2} = -0.174$, $\lambda^{(2)}_{k^2} = -0.422$, $\lambda^{A}_{\zeta} = -0.0138 \times (2\pi/a)^2$, and $\lambda^{B}_{\zeta} = 0.0885 \times (2\pi/a)^2$, $\lambda^{A}_{k\xi} = 0.0408 \times (2\pi/a)$, and $\lambda^{B}_{k\xi} = -0.0954 \times (2\pi/a)$. The parameters $\lambda^{A}_{\zeta^2}$, $\lambda^{B}_{\zeta^2}$, and $\lambda^{AB}_{\zeta^2}$ exhibit slow convergence, but are irrelevant if ζ_A and ζ_B are small enough.
[27] Y. Hatsugai, Phys. Rev. Lett. **71**, 3697 (1993)
[28] K. Wakabayashi, Y. Takane, and M. Sigrist, Phys. Rev.

Lett. **99**, 036601 (2007)
[29] X. Huang, Y. Lai, Z. H. Hang, H. Zheng, and C. T. Chan, Nature Materials **10**, 582 (2011)
[30] M. Oshikawa, Phys. Rev. B **50**, 17357 (1994)
[31] This "local" procedure does not correctly take account of the entire first Brillouin zone, which is two-torus. See discussions in Ref. 30.
[32] For completeness, the parameters of the effective Hamiltonian are $\lambda^{(1)}_{k^2} = -0.174$, $\lambda^{(2)}_{k^2} = -0.422$, $\lambda^A_\zeta = -0.0138 \times (2\pi/a)^2$, and $\lambda^B_\zeta = 0.0885 \times (2\pi/a)^2$, $\lambda^A_{k\xi} = 0.0408 \times (2\pi/a)$, and $\lambda^B_{k\xi} = -0.0954 \times (2\pi/a)$. The parameters $\lambda^A_{\zeta^2}$, $\lambda^B_{\zeta^2}$, and $\lambda^{AB}_{\zeta^2}$ exhibit slow convergence, but are irrelevant if ζ_A and ζ_B are small enough.